Bioactive Materials 5 (2020) 980–989

Contents lists available at ScienceDirect

Bioactive Materials

journal homepage: http://www.keaipublishing.com/biomat

Comparing the regeneration potential between PLLA/Aragonite and PLLA/Vaterite pearl composite scaffolds in rabbit radius segmental bone defects

Qianli Huang[a,*], Yuansheng Liu[b,c], Zhengxiao Ouyang[d], Qingling Feng[b,**]

[a] State Key Laboratory of Powder Metallurgy, Central South University, Changsha, 410083, PR China
[b] State Key Laboratory of New Ceramics and Fine Processing, School of Materials Science and Engineering, Tsinghua University, Beijing, 100084, PR China
[c] Public Security College, Northwest University of Political Science and Law, Xi'an, 710122, PR China
[d] Department of Orthopedics, The Second Xiangya Hospital, Central South University, Changsha, 410083, PR China

ARTICLE INFO

Keywords:
Composite scaffold
Aragonite
Vaterite
Segmental bone defect
Bone regeneration

ABSTRACT

Mussel-derived nacre and pearl, which are natural composites composed $CaCO_3$ platelets and interplatelet organic matrix, have recently gained interest due to their osteogenic potential. The crystal form of $CaCO_3$ could be either aragonite or vaterite depending on the characteristics of mineralization template within pearls. So far, little attention has been paid on the different osteogenic capacities between aragonite and vaterite pearl. In the current work, aragonite or vaterite pearl powders were incorporated into poly-L-lactic acid (PLLA) scaffold as bio-functional fillers for enhanced osteogenesis. *In intro* results revealed that PLLA/aragonite scaffold possessed stronger stimulatory effect on SaOS-2 cell proliferation and differentiation, evidenced by the enhanced cell viability, alkaline phosphatase activity, collagen synthesis and gene expressions of osteogenic markers including osteocalcin, osteopotin and bone sialoprotein. The bone regeneration potential of various scaffolds was evaluated *in vivo* employing a rabbit critical-sized radial bone defect model. The X-ray and micro-CT results showed that significant bone regeneration and bridging were achieved in defects implanted with composite scaffolds, while less bone formation and non-bridging were found for pure PLLA group. Histological evaluation using Masson's trichrome and hematoxylin/eosin (H&E) staining indicated a typical endochondral bone formation process conducted at defect sites treated with composite scaffolds. Through three-point bending test, the limbs implanted with PLLA/aragonite scaffold were found to bear significantly higher bending load compared to other two groups. Together, it is suggested that aragonite pearl has superior osteogenic capacity over vaterite pearl and PLLA/aragonite scaffold can be employed as a potential bone graft for bone regeneration.

1. Introduction

Large bone defects caused by various bone diseases such as severe trauma, tumor resection or bone infection have long been grand challenges worldwide due to their weak capacity to self-regenerate [1]. Clinically, autografts originated from fibula, ilium and rib are perceived as gold standard for small bone defects owing to their outstanding osteoconductivity and osteoinductivity. However, the donor shortage and donor site mobility severely restrict the therapeutic use of autografts for large bone defects [2]. Allografts are commonly regarded as a suboptimal option compared to autografts, while they have risks in raising uncontrollable immune response and transmitting disease [3]. Therefore, there is a strong clinical demand in the development of advanced synthetic bone substitutes with high therapeutic efficacy as alternatives to autologous and allogous grafts.

Bone tissue engineering (BTE) is a promising approach for large bone defect treatment [4]. In BTE, a critical challenge is to develop a proper three dimensional (3D) porous scaffold which can be acellular or cells/drugs-loaded as a temporary matrix for bone in-growth and regeneration [5]. An ideal scaffold should be capable of supporting or promoting cell adhesion, proliferation and differentiation as well as vascularization and osteointegration [6]. Currently used biomaterials for BTE scaffolds can be roughly divided into three types including bioactive ceramics, degradable polymers and composites [7]. Bioceramics such as hydroxyapatite (HA), tri-calcium phosphate (TCP) and bioactive glasses (BG) have favorable biocompatibility and osteoconductivity, whereas they are rarely used alone as scaffold materials due to their brittleness and difficulty for processing [8–10]. Synthetic

Peer review under responsibility of KeAi Communications Co., Ltd.
* Corresponding author.
** Corresponding author.
E-mail addresses: hql1990@163.com (Q. Huang), biomater@mail.tsinghua.edu.cn (Q. Feng).

https://doi.org/10.1016/j.bioactmat.2020.06.018
Received 7 May 2020; Received in revised form 9 June 2020; Accepted 27 June 2020

polymers such as poly-lactic acid (PLA), poly-glycolic acid (PGA) and their copolymers (PLGA) have been extensively used in BTE field due to their controllable degradation rates and easiness in scaffold forming [11,12]. However, these synthetic polymers have drawbacks such as poor bioactivity and low ability to interact with cells. Thus, composite scaffolds with polymers as matrices and bioactive ceramics as functional fillers have been widely developed in order to take advantages of the favorable osteoconductivity of bio-ceramics and adjustable degradability of polymers [13–15]. Unfortunately, current polymer/bioceramic composite scaffolds are still found to be insufficiently osteoinductive. Hence, growth factors such as bone morphogenetic proteins (BMPs) and vascular endothelial growth factors (VEGFs) have been reported to be further loaded into the scaffold systems for enhanced bone regeneration [16–18]. However, the high cost and short half-life are considered as two major limitations for the extensive applications of these growth factors clinically.

Similar to bone, nacre and pearl are natural composite materials consisting of highly ordered calcium carbonate crystals (~95 wt%) cemented by an organic matrix (~5 wt%), exhibiting a typical 'brick and mortar' microstructure [19]. There are *in vitro* and *in vivo* evidences showing the osteogenic potential of nacre. Lopez et al. found that nacre could lead to the formation of bone-like nodules induced by human osteoblasts [20]. Green et al. reported that human bone marrow-derived stromal cells (hBMSCs) co-cultured with nacre chips expressed higher alkaline phosphatase (ALP) activity compared to the control group treated by BMP-2, indicating the osteoinductive potential of nacre [21]. In an *in vivo* case, nacre powders mixed with autologous blood were injected between the fifth and sixth lumbar vertebrae of rabbits. The results showed that nacre could induce endocontrodral bone formation like autografts and the spinal fusion was achieved by 5 weeks [22]. In another case, blood-mixed nacre powders were injected into the bone missing area of human upper jaw. After 6 months, osteoblast activation and new bone formation were observed throughout the implant material [23]. Although the exact mechanism by which nacre promotes bone regeneration still remains veiled, scientists have speculated that the organic component of nacre may contain water soluble signal molecules that can stimulate osteogenesis. Bedouet et al. reported that small molecules (< 1 kDa), especially peptides, were prevalent in nacre [24]. Lamghari et al. found that the stimulatory effect of nacre water soluble matrix (WSM) on BMSCs was similar to that of tumor growth factor-β (TGF-β) and BMPs [25]. Rousseau et al. suggested that WSM of nacre had higher efficacy in accelerating osteoblastic differentiation than dexamethasone [26]. In general, nacre is considered to be promising for BTE applications due to its favorable osteogenic capacity. Moreover, the osteogenic signal molecules reside in nacre could be potential alternatives for those expensive growth factors.

As nacre and pearl are non-porous as well as difficult to mold and degrade, their powders are commonly used as functional fillers in 3D porous composite scaffolds. In recent years, several kinds of nacre- or pearl-containing composite scaffolds have been developed through different techniques [27]. Xu et al. employed low-temperature deposition manufacturing to fabricate PLGA/pearl composite scaffold. The pearl/PLGA scaffold promoted the ALP activity, collagen I (Col-I) synthesis in marrow stem cells (MSCs) *in vitro* compared to PLGA/TCP scaffold [28]. Yang et al. reported that PLGA/pearl composite scaffold fabricated by gel casting and salt leaching method could promote the growth of osteoblasts *in vitro* compared to PLGA control [29]. Zhang et al. developed poly-caprolactone (PCL)/pearl scaffold using 3D printing technique. The proliferation, ALP activity and bone related gene expressions such as osteocalcin (OCN), bone sialoprotein (BSP), BMP-2 and Col-I were significantly enhanced in osteoblasts cultured on PCL/pearl scaffold compared to PCL control [30]. These previous works highlighted the benefit of using pearl powders as functional fillers in BTE composite scaffolds. However, they also ignored that calcium carbonate has three different crystal forms including aragonite, vaterite and calcite. Among them, calcite is the most stable polymorph, while vaterite is the most unstable one. Li et al. reported that calcite nanoparticles promoted osteogenesis compared to adipogenesis in human MSCs [31]. Fricain et al. found that the proliferation and protein expressions of MSCs were comparable on aragonite and calcite, suggesting the similar osteogenic performances of these two $CaCO_3$ polymorphs [32]. So far, the synthesis of pure vaterite phase without using organic template for mineralization still remains as a huge challenge due to the high instability of vaterite under room temperature and atmospheric pressure. Moreover, inorganic calcite easily transforms to aragonite (> 60 °C) or calcite (< 60 °C) once it is exposed to water [33]. Thus, it is difficult to directly compare the osteogenic capacities between pure aragonite and vaterite. It is speculated that aragonite and vaterite may possess various osteogenic capacities due to their different degradation rates. For pearls, the inorganic component of the lustrous ones is characterized to be aragonite, while that of non-lustrous ones is pure vaterite [34]. The existing form of calcium carbonate is directly related to the composition of organic component in pearl [35]. In our previous works, poly-L-lactic acid (PLLA)/aragonite pearl and PLLA/vaterite pearl scaffolds were successfully prepared by thermally induced phase separation method [36,37]. Compared to pure PLLA scaffold, composite scaffolds incorporated with aragonite or vaterite pearl powders exhibited enhanced compressive strength and modulus [36]. Moreover, the PLLA/aragonite pearl scaffold was found to exhibit stronger stimulatory effect on the proliferation and ALP activity of MSCs compared to PLLA/vaterite pearl scaffold [36]. It is considered to be related to the different organic matrices and degradation rates of these two kinds of pearl powders. So far, the *in vivo* performances of pearl-containing composite scaffolds still remain to be explored.

Hence, the aim of the current work is to systematically evaluate the biological performances of PLLA/aragonite pearl and PLLA/vaterite pearl composite scaffolds both *in vitro* and *in vivo*. Human osteoblastic SaOS-2 cells and New Zealand white rabbits were employed as cell and animal model, respectively. For comparison, pure PLLA scaffold was also prepared.

2. Experimental procedure

2.1. Scaffold preparation

The scaffolds were prepared by thermally induced phase separation and subsequent freeze-drying as previously reported [36]. Briefly, PLLA with molecule weight of 17.9×10^4 Da (Shandong Medical Device Company, China) was dissolved in 1, 4-dioxane at a mass-to-volume ratio of 5% (g/mL) by stirring for 8 h at room temperature. Thereafter, aragonite or vaterite pear powders (~17.5 μm) prepared by mechanical grounding using a grinder were added into the PLLA solution at a mass-to-mass ratio of 20%. After being further stirred for 15 min, the mixture was sonicated for 30 min. Subsequently, the mixture was casted into cylinder-shaped molds (for in *vitro* tests: 15 mm in diameter and 100 mm in length; for *in vivo* tests: 3 mm in diameter and 10 mm in length) and frozen for 24 h at −20 °C. Then, the lyophilization process was carried out for 48 h at −60 °C. The pure PLLA scaffolds were prepared as described above without the addition of pearl powders. The specimens are denoted as PLLA/aragonite or PLLA/vaterite scaffolds depending on the type of added pearl powders.

2.2. Scaffold characterization

The specimen microstructure was analyzed by scanning electron microscopy (SEM; FEI Quanta 250FEG, USA). The chemical composition of specimens was evaluated with X-ray photoelectron spectromety (XPS; Thermo Scientific Escalab 250Xi, UK). The binding energy of C 1s (284.8 eV) in CH_2 group was used to calibrate the spectra.

2.3. Cell culture and seeding

Human osteoblastic SaOS-2 cells were incubated in McCoy's medium containing 15% fetal bovine serum (FBS) and 1% antibiotics (100 U/mL penicillin and 100 μg/mL streptomycin) under standard condition (37 °C, 5% CO_2 and 100% humidity). The culture medium was changed every other day until about 90% confluence was reached.

Before cell seeding, the specimens were cut into discs (15 mm in diameter and 1 mm in thickness) and disinfected using a cobalt-60 source (dose rate: 8 kGy). The sterilized specimens were then placed into 24-well plate and pre-soaked in McCoy's complete culture medium for 24 h. Subsequently, 1 mL complete culture medium containing 3×10^4 SaOS-2 cells were dropped onto the surface of each specimen.

2.4. Cell morphology and proliferation

For SEM observation, the cells were fixed with 2.5% glutaraldehyde solution for 12 h and then dehydrated in ethanol solutions with ascending concentrations (from 20 to 100%, 10 min at each concentration). Subsequently, the intracellular ethanol was substituted using a series of graded tertiary butanol solutions (from 25 to 100% in ethanol, 10 min at each concentration). After freeze drying, the specimens were gold sputtered and analyzed employing SEM.

The proliferation of SaOS-2 cells was determined by Cell Counting Kit-8 (CCK-8, Dojindo, Japan). At each time point, 270 μL of culture medium and 30 μL of CCK-8 solution were added into each well and then incubated for 1 h at 37 °C. Finally, the optical density values of solutions were measured using a microplate analyzer (PerkinElmer, USA) at 450 nm.

2.5. ALP activity and collagen (Col) secretion

For qualitative analysis of ALP activity, the specimens were fixed in 4% paraformaldehyde and stained with BCIP/NBT alkaline phosphatase color development kit (Beyotime, China). For ALP activity quantitative assessment, the cells were lysed in 0.2% Triton X-100. The ALP activity in lysates was determined employing an ALP detection kit (Jiancheng, China) and normalized by the total protein content measured by a BCA assay kit (Beyotime, China).

For the measurement of Col synthesis, the cells were fixed and then stained with sirius red (Solarbio, USA) with a concentration of 0.1% at room temperature for 12 h. The stained specimens were washed and photographed. Thereafter, the dyes were dissolved in 0.2 M NaOH/methanol (volume-to-volume ratio = 1:1) for quantitative analysis. The optical density values of solutions were determined by a microplate analyzer at 570 nm.

2.6. In vitro mineralization

To facilitate mineralization, osteogenic inducers including ascorbic acid (50 μg/mL), dexamethasone (10 nM) and β-glycerophosphate (10 mM) were added into normal culture medium. After culturing SaOS-2 cells in osteogenic medium for 14 days, the specimens were treated as described in section 2.4 for SEM sample preparation. Thereafter, the deposited minerals were analyzed employing SEM equipped with an energy dispersive X-ray spectroscopy (EDS) system.

2.7. Gene expressions

The osteogenic gene expressions including osteocalcin (OCN), osteopotin (OPN) and bone sialoprotein (BSP) in SaOS-2 cells cultured on various specimens were analyzed by real time polymerase chain reaction (RT-PCR) assay. After culturing for 3 days, total RNA was extracted using Trizol reagent from cells. The concentration of RNA was measured by a NanoDrop spectrophotometer (Thermo Fisher Scientific, USA). First standard complementary DNA (cDNA) was synthesized from total RNA using Fast-Quant RT kit (Tiangen, China) following manufacturer's instructions. The RT-PCR analysis was performed on a CFX96 Touch RT-PCR Detection System (Bio-Rad, USA) using SYBR Green detection reagent (Bio-Rad, USA). The 2-ΔΔCT method was used to analyze data. Table S1 listed the primers used for SaOS-2 cells in the current work.

2.8. Surgical procedure

Bilateral critical-sized segmental radial bone defect model in adult rabbits was employed in the current work. The animal experimentation was approved by the Ethics Committee of the Second Xiangya Hospital of Central South University. In brief, twenty-four male New Zealand white rabbits (6-month-old) with an average weight between 2.5 and 3.0 kg were used. Four experimental groups were specified including blank, PLLA, PLLA/aragonite and PLLA/vaterite. The rabbits were anaesthetized with ear intravenous injection of 3% pentobarbital sodium solution (30 mg/kg). Subsequently, bilateral forelimbs of rabbits were shaved and washed with 70% ethanol. After muscle dissection and radius exposure, a segmental defect of 10 mm was created in the middle of radial bone using a dental bur. The periosteum was removed to reduce the spontaneous regeneration potential of defects. The radius defects were either grafted with as-prepared cylinder scaffolds or left blank. No additional fixation was employed for the forelimbs. Finally, the wounds were closed by suturing. The rabbits were housed separately in cages and each was given penicillin at a dose of 4×10^4 units per day for 5 days post-surgery. The animals were sacrificed successively at week 4, 8 and 12 to obtain their bony tissues.

2.9. X-ray examination

Immediately after sacrificing the animals, standardized radiographs were performed on the experimental limbs. The images were evaluated according to the Lane-Sandhu radiographic scoring system (SI Table 2) to score defect bridging as well as bone formation and modeling [38].

2.10. Micro-computed tomography (micro-CT) analysis and biomechanical evaluation

After X-ray examination, the bony specimens were employed for micro-CT evaluation before mechanical testing or histological analysis. The specimens were scanned using SIEMENS Inveon MMCT micro-CT instrument with voltage and power set as 55 kV and 80 W, respectively. The resolution of imaging was 20 μm in the current work. Using Inveon Acquisition Workplace software, the region of interest (ROI) was chosen as a cylinder area (10 mm in hight) covering the defect created during surgery for quantitative analysis of bone volume/total volume (BV/TV), trabecular number (Tb.Nu), trabecular thickness (Tb·Th) and trabecular separation (Tb.Sp). The biomechanical properties of bony specimens were measured by three-point bending test.

2.11. Histological analysis

The bony specimens were fixed with 10% formaldehyde solution and decalcified in 12.5% EDTA. After complete decalcification and dehydration, the specimens were embedded in paraffin and cut into 5 mm serial sections. The sections were stained with hematoxylin/eosin (H&E) or Masson's trichrome method and subsequently photographed using optical microscopy. It is worthy of mentioning that light green (0.5 g light green in 100 mL distilled water) was employed for collagen fiber staining in the process of Masson's trichrome staining.

2.12. Statistical analysis

Results were shown as mean ± standard deviation (SD). All data were generated from three or four independent experiments. Statistical

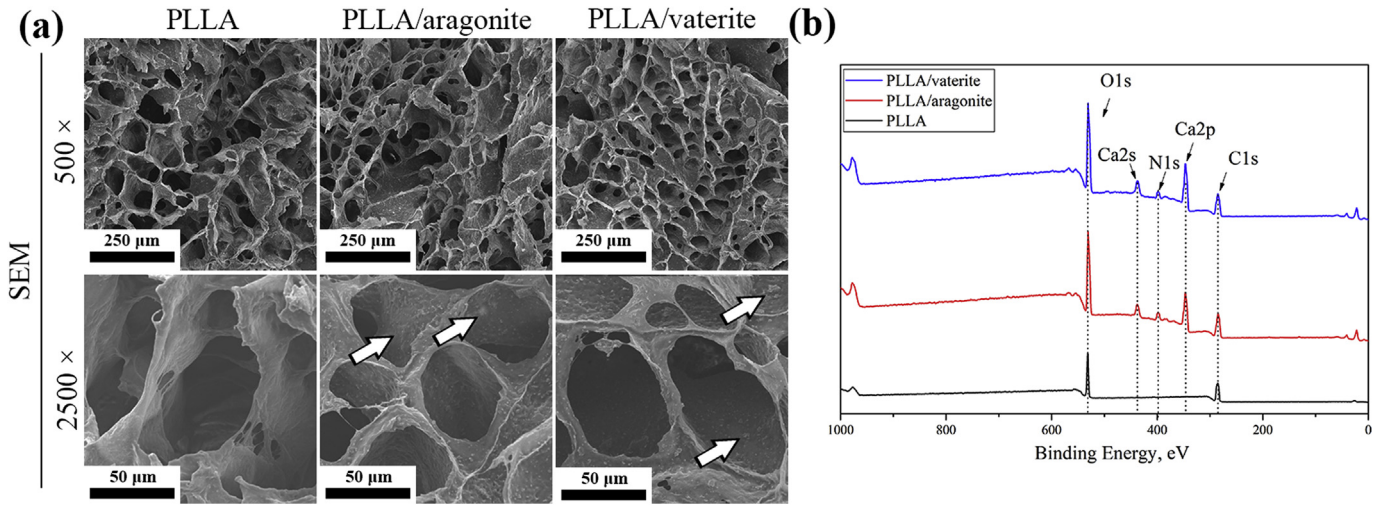

Fig. 1. (a) The SEM images of various scaffolds and (b) their relevant XPS spectra. The white arrows showed the presence of pearl powders within composite scaffolds.

analysis was conducted employing one-way analysis of variance (ANOVA) followed by post hoc tests. A value of $p < 0.05$ was considered to be significant.

3. Results and discussions

3.1. Characterizations of scaffolds

As shown in Fig. 1, all PLLA-based scaffolds exhibited a similar macro-porous microstructure. At a low magnification (500 ×), it was found that interconnected pores with sizes ranging from 50 to 150 μm were homogeneously distributed in scaffold matrices. The pores exhibited a ladder-like morphology due to the directional crystallization of solvent during freezing. At a high magnification (2500 ×), morphological differences were noticed between various groups. For PLLA group, the scaffold surface was relatively smooth. However, the surfaces of composite scaffolds were found to be rougher owing to the presence of evenly distributed pearl powders (indicated by the white arrows). Scaffolds with pore sizes ranging from 20 to 1500 μm were previously reported to be used for BTE applications [39–41]. Commonly, small pores (100–150 μm) are considered to be critical for nutrition transport and cell infiltration [42]. Larger pores (> 300 μm) were found to be required for substantial bone in-growth [41]. Thus, the initial pores of scaffolds in the current work were not large enough for long-term bone in-growth. The degradation of scaffolds after implantation is considered to be essential for the formation of larger pores that support bone regeneration.

The chemical compositions of specimens were explored by XPS technique. Consistent with the composition of PLLA, only C and O signals were detected for PLLA scaffold (Fig. 1b). For composite scaffolds, additional elements including Ca and N were detected. The element Ca was attributed to the presence of inorganic component $CaCO_3$ and N was corresponding to the peptide $–NH_2$ group within pearl [43]. According to our previous work, the content of WSM in aragonite pearl (~1.02 wt%) was higher than that in vaterite pearl (~0.79 wt%). However, aragonite pearl contained less acid soluble matrix (ASM) and acid insoluble matrix (AIM) than vaterite pearl [35]. As differences in the organic components of aragonite and vaterite pearls are speculated to lead to various osteogenesis, the biological performances of composite scaffolds were assessed both *in vitro* and *in vivo*.

3.2. In vitro biological performance

3.2.1. Osteobalst morphology and proliferation

The morphology and proliferation of SaOS-2 cells on various scaffolds were investigated by SEM visualization and CCK-8 test, respectively. As shown in Fig. 2a, the cells exhibited a roundish morphology following the initial attachment onto scaffolds for 1 day. The cells were more flattened on composite scaffold surfaces compared to those on PLLA scaffold. On day 3, further spreading and cytoskeleton extension were noticed for cells attached on all scaffold surfaces. The cells continued to proliferate and more cells were observed on day 5. On PLLA/aragonite scaffold surface, the cells reached almost confluence and cell borders became indistinguishable. Consistent with SEM observation, the CCK-8 results showed that PLLA/aragonite scaffold stimulated the proliferation of SaOS-2 cells compared to the other two groups (Fig. 2b). Compared to PLLA scaffold, PLLA/vaterite scaffold support the growth of cells without showing significant stimulatory effect.

3.2.2. Osteoblast differentiation

The differentiation of SaOS-2 cells grown on various scaffolds for different durations was evaluated. As shown in Fig. 3a, PLLA/aragonite scaffold promoted the ALP activity of SaOS-2 cells compared to the other two groups on both day 4 and 7. The Col productions in SaOS-2 cells on day 5 and 10 were in the following order: PLLA/aragonite > PLLA/vaterite > PLLA (Fig. 3b). After culturing SaOS-2 cells on PLLA/aragonite scaffold for 14 days with the supplement of mineralization inducers, the formation of bone-like nodules was observed on the surface of PLLA/aragonite scaffold (Fig. 3c, indicated by the white arrows). The nodules were consisted of nano-crystals with an average size of 20 nm. As shown in Fig. 3d, elemental signals of C, Ca, O, P and Na were detected for the nodules, indicating that the nodules were Ca- and P-containing minerals. However, the formation of bone-like nodules was rarely found on PLLA or PLLA/vaterite scaffold (SI Fig. 1). The osteogenic gene expressions were evaluated by RT-PCR technique. As shown in Fig. 3e, composite scaffolds up-regulated the gene expressions of OCN, OPN and BSP compared to PLLA scaffold in general, although the BSP gene expressions were comparable between PLLA and PLLA/vaterite group. Compared to those in PLLA/vaterite group, the levels of OCN and OPN expressions were significantly higher in PLLA/aragonite group. Together, the results suggest that incorporating pearl powders (aragonite or vaterite) into PLLA scaffold could lead to enhanced differentiation of SaOS-2 cells *in vitro*. The stimulatory effect was found to be stronger in PLLA/aragonite group compared to PLLA/vaterite group. In our previous work, the ALP

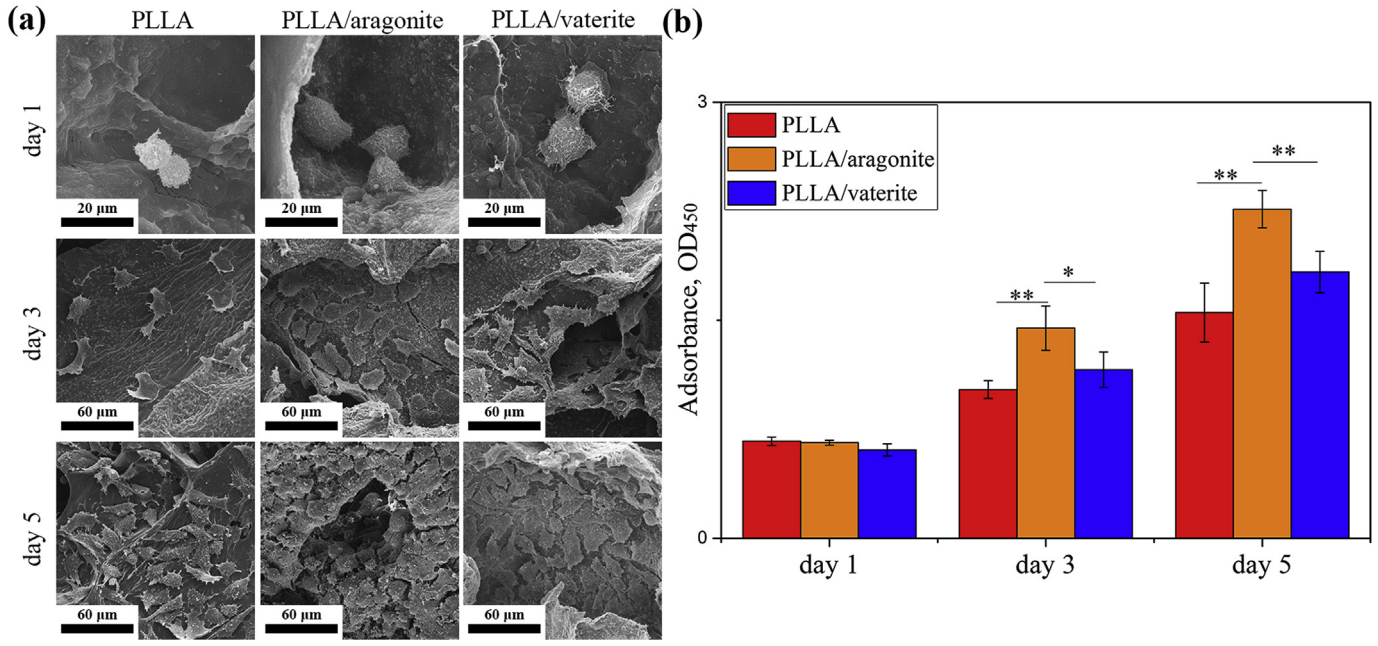

Fig. 2. (a) The SEM images of SaOS-2 cells grown on various scaffolds for 1, 3 and 5 days as well as (b) relevant cell proliferation behaviors evaluated by CCK-8 assay. *p < 0.05 and **p < 0.01.

activity of MSCs was promoted by PLLA/aragonite scaffold, while slightly inhibited by PLLA/vaterite scaffold [36]. This inconsistency is considered to be caused by the usage of different cellular types.

3.3. In vivo biological performance

Critical-sized bone defects are of great importance for the evaluation of osteogenic potential of BTE scaffolds. Hollinger et al. suggested that the defect of long cannular bone could not heal spontaneously when defect size-to-bone diameter ratio was larger than 1.5 [44]. Commonly, the radius diameter of rabbits is in the range of 3–4 mm. According to previous literatures, radius defects with sizes ranging from 10 to 20 mm were described as being of critical size for rabbits [45,46]. Zhou et al. reported that the rabbit radius defect with a size of 10 mm could maintain its size throughout a 12-week period after the removal of periosteum [47]. To investigate the *in vivo* bone regeneration capacity of PLLA/pearl powders composite scaffolds, a rabbit critical-sized segmental radial bone defect model was employed in the current work (Fig. 4a).

3.3.1. Radiography

As shown in Fig. 4b, the formation of new bone was non-obvious in all groups at week 4. Tiny bone callus formed at the end of bone defect was noticed in PLLA group at week 8, while distinct formation of bone callus was found in the osteotomy gaps implanted with composite scaffolds. At week 12, the defect of PLLA group was filled with newly formed bone callus without reaching bridging, while the defects in the composite scaffold groups were bridged with new bone. The radiograph density of defect in PLLA/aragonite group was found to be larger than that in PLLA/vaterite group. The osteotomy gap was still obviously visible in the blank control group at week 12 (Fig. 4b). As shown in Fig. 4c, the Lane-Sandhu scoring system was employed to evaluate the conditions of bone bridging and formation in defects implanted with scaffolds. At week 4, the scores were comparable for all groups. With

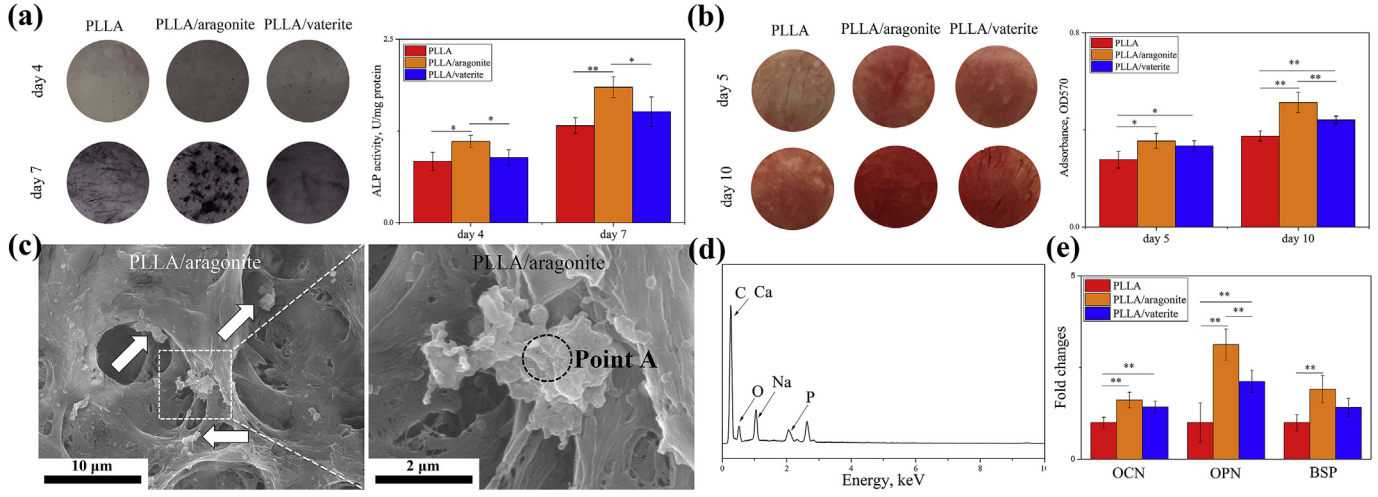

Fig. 3. (a) The ALP activity, (b) Col synthesis of SaOS-2 cells cultured on various surfaces for different durations. (c) *In vitro* mineralization of SaOS-2 cells grown on PLLA/aragonite scaffold for 14 days and (d) EDS elemental analysis of the mineral deposits (point A). The gene expressions of osteogenic markers including OCN, OPN and BSP evaluated by RT-PCR technique on day 3. *p < 0.05 and **p < 0.01.

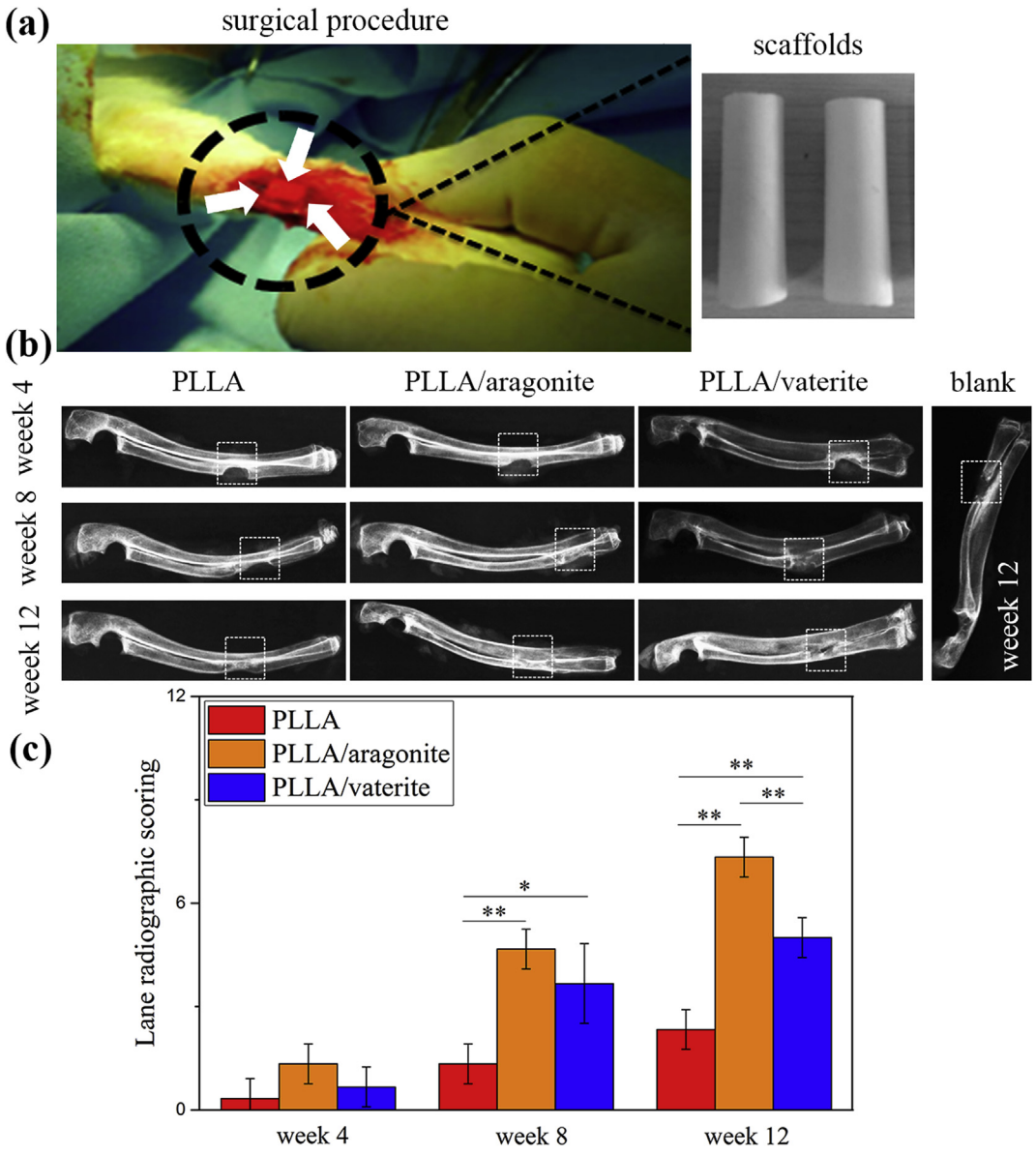

Fig. 4. (a) The surgical procedure and macroscopic morphology of scaffolds. (b) The digital radiographs and (c) Lane-Sandhu radiographic scores of rabbit radius defects implant with various scaffolds at week 4, 8 and 12 post-surgery. *p < 0.05 and **p < 0.01.

prolonged durations (week 8 and 12), the scores of various groups were basically in the following trend: PLLA/aragonite > PLLA/vaterite > PLLA, although there was no statistically significant difference between the scores in PLLA/aragonite and PLLA/vaterite groups at week 8.

3.3.2. Micro-CT evaluation

Compared to the scoring of radiographs, 3D reconstructed micro-CT images allowed for a more precise assessment of new bone formation within the osteotomy gaps. As shown in Fig. 5a, more newly formed trabecular bone tissues were observed in defects of composite scaffold groups compared to PLLA group at week 8. Till week 12, obvious bone bridging was noticed in both groups implanted with composite scaffolds, indicating the true osteoconductive nature of composite scaffolds. Compared to PLLA/vaterite group, a relatively more intact radius contour was formed in PLLA/aragonite group. However, the bridging of defect in PLLA group was atypical at week 12, which could be regarded as non-bridging. As shown in Fig. 5b–e, quantitative histograms of bone formation were obtained. At week 8, the bone regeneration performance of various groups basically followed the trend: PLLA/aragonite > PLLA/vaterite > PLLA. At week 12, the values of BV/TV and Tb.Nu were comparable for composites scaffolds and higher than those of PLLA scaffold (Fig. 5b and d). The PLLA/aragonite group still possessed smaller Tb.Sp value compared to PLLA/vaterite group at week 12 (Fig. 5e). However, the Tb·Th values reached the same level for all groups without showing statistically significant difference (Fig. 5c). In general, the micro-CT results revealed that composite scaffolds exhibited better bone healing performances compared to pure PLLA scaffold.

3.3.3. Histological analysis

To further evaluate the healing process of bone defects in various groups. H&E (SI Fig. 2) and Masson's trichrome (Fig. 6) staining were performed at week 4, 8 and 12 post-surgery. As shown in Fig. 6, a typical endochondral bone formation process was revealed by Masson's trichrome staining. The theory of endochondral bone formation could be divided into three stages including inflammation and cartilage formation (initial stage), primary bone formation (secondary stage) and bone remodeling (maturation stage) [17]. For the initial stage, the inflammatory cells presented at bone defect site release various kinds of cytokines to raise an acute inflammatory response and simultaneously

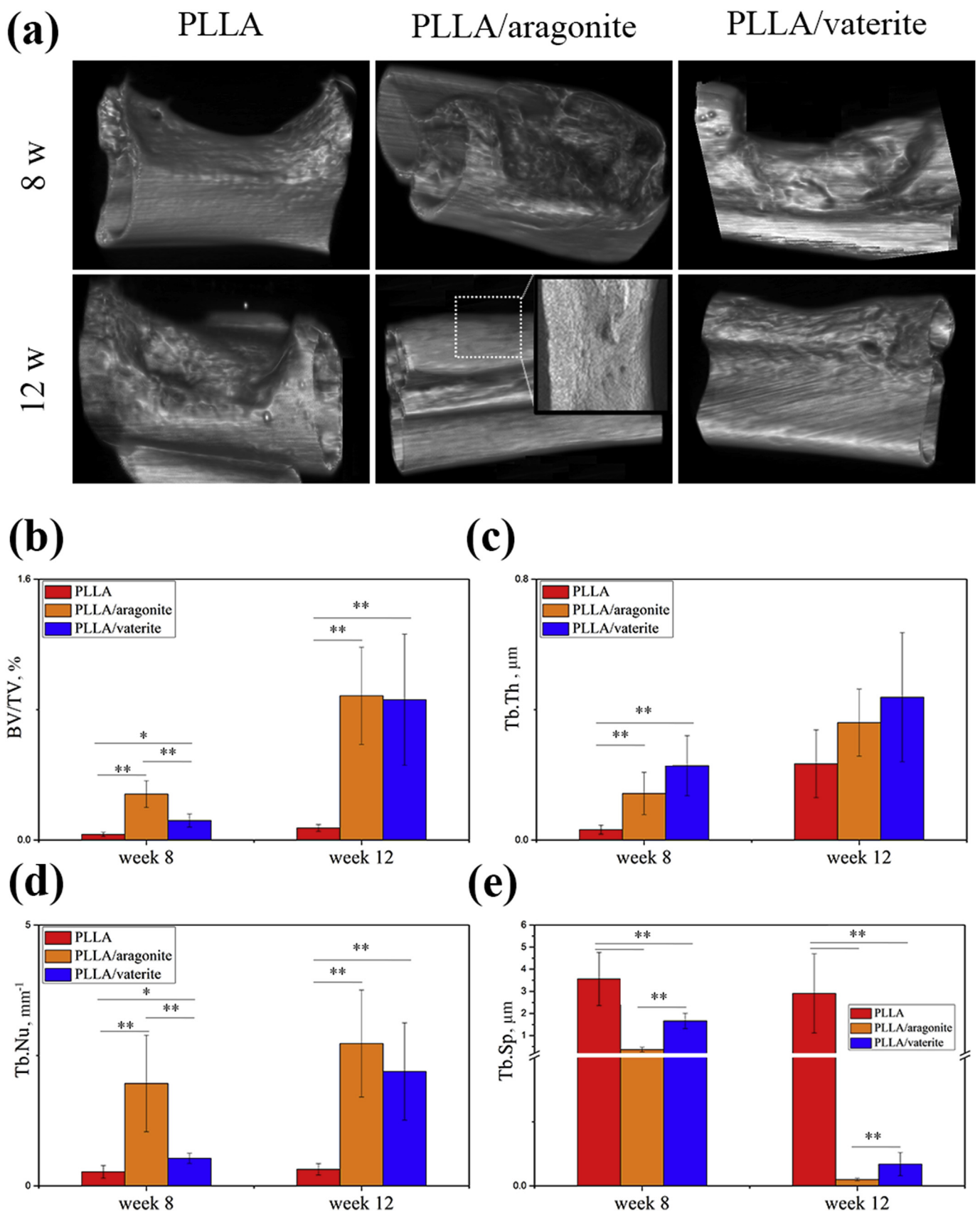

Fig. 5. (a) The micro-CT analysis of different groups at week 8 and 12 as well as quantitative parameters of defect healing process obtained from micro-CT images: (b) BV/TV; (c) Tb·Th; (d) Tb.Nu and (e) Tb·Sp. *$p < 0.05$ and **$p < 0.01$.

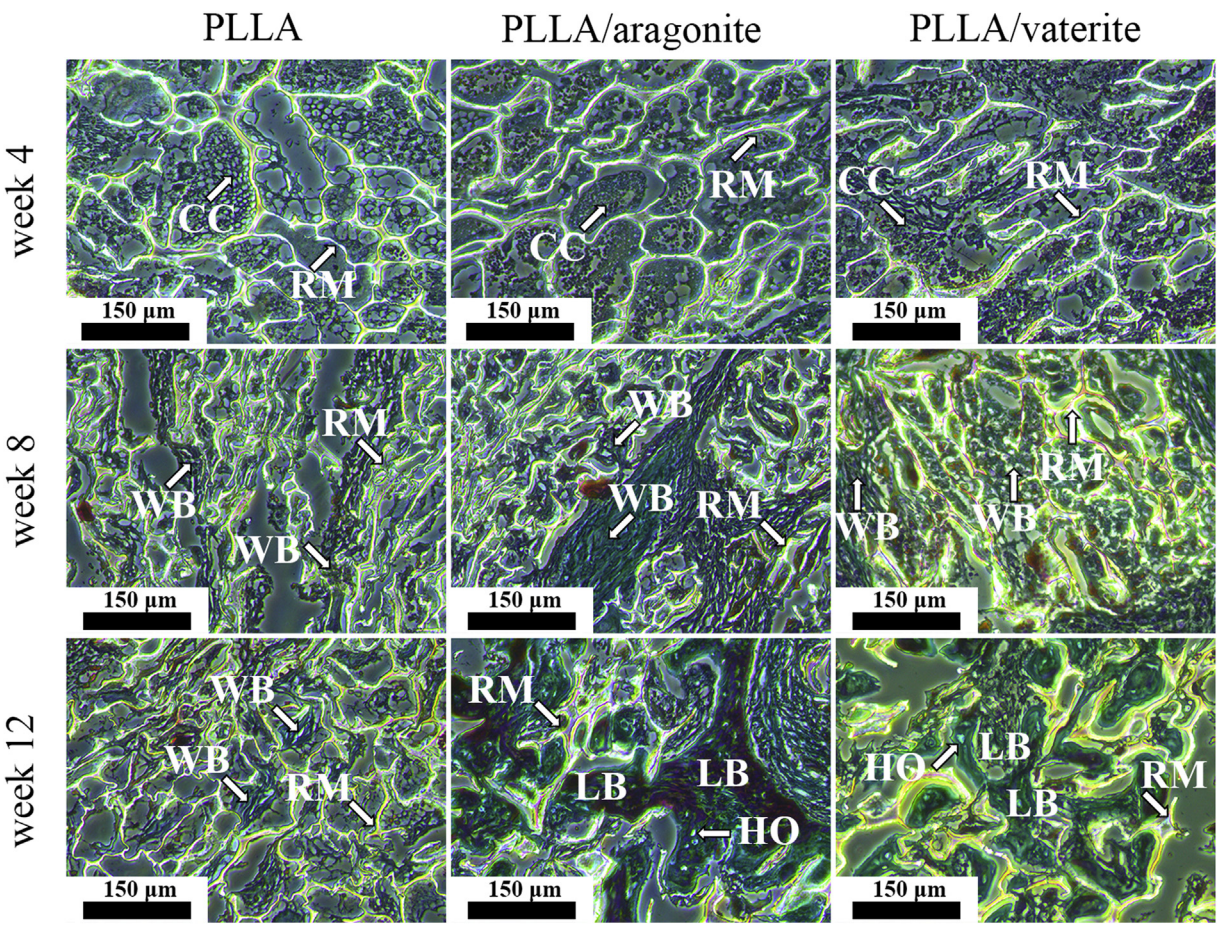

Fig. 6. The histological micrographs of Masson's trichrome staining of bone defects in each group at week 4, 8 and 12 post-surgery. RM, CC, WB, LB and HO were denoted for residual materials, chondrocytes, woven bone, lamellar bone and Haversian osteons, respectively.

recruit MSCs towards the defect site. The recruited MSCs subsequently differentiate into chondrocytes and form cartilage. For the secondary stage, the cartilage transforms to woven bone through the osteogenic activity of osteoblasts. Finally, the woven bone undergoes remodeling and gradually turns into matured lamellar bone. In the current work, the pores of scaffolds were infiltrated with abundant chondrocytes at week 4. The formation of woven bone was observed in all groups at week 8. Compared to the other two groups, PLLA/aragonite scaffold resulted in enhanced woven bone formation. Till week 12, the woven bone transformed to lamellar bone in PLLA/aragonite and PLLA/vaterite group. Typical Haversian osteons with a ring-like structure were observed within the lamellar bone tissue. The maturity of lamellar bone in PLLA/aragonite group was significantly higher than that in PLLA/vaterite group. However, the formation of lamellar bone was not observed in PLLA group. Similarly, Lamghari et al. reported that nacre powders induced spinal fusion of rabbits *in vivo* by endochondral bone formation [22]. The degradation of scaffolds was noticed in all groups although complete degradation was not achieved till week 12. Consistently, Walton reported that the presence of PLLA *in vivo* even after implantation for 3 years [48]. Thus, PLGA is more recommended to be used as scaffold material compared to PLLA as its degradation rate can be largely controlled by adjusting the ratio between PLA and PGA [49]. It is well-known that PLLA degrades by hydrolytic cleavage of its polymer chains [50]. The acidic micro-environment created by proton release may lead to emergence of chronic inflammation [51]. However, no obvious inflammation was noticed in the current work, indicating that the effect of acidity could be neglected for highly porous PLLA scaffold. For composite scaffolds, the degradation of pearl powders could raise the environmental pH to some extent and neutralize the protons released by PLLA [37].

3.3.4. Biomechanical evaluation

For rabbit limbs, a load is commonly shared by the syndesmosis between radius and ulna. Guda et al. suggested that the radius and ulna should be considered as a unit in the physiological setting [52]. It is considered to be more biologically-relevant to conduct the biomechanical test on them together. Thus, the radius was not separated from the ulna for three-point bending test in the current work (Fig. 7a). As shown in Fig. 7b, the values of maximum bending load were comparable for various groups at week 4. The PLLA/aragonite group could bear significantly larger bending load compared to other two groups at week 8 and 12. No significant difference was found between the PLLA and PLLA/vaterite group throughout a 12-week period of time.

In this study, aragonite or vaterite pearl powders were added into PLLA scaffold as functional fillers. The biological performances of as-fabricated composite scaffolds were systematically evaluated both *in vitro* and *in vivo*. According to the results presented in this work, the composite scaffolds were found to exhibit enhanced osteogenic capacity compared to pure PLLA scaffold. Moreover, PLLA/aragonite scaffold possessed stronger stimulatory effect on bone regeneration compared to PLLA/vaterite scaffold. The underlying mechanism of the stimulatory effect of PLLA/aragonite scaffold on bone healing is still an open question, to which some ideas might be provided here by combining current theories with our findings. As pearl is a composite material composed of inorganic $CaCO_3$ and organic matrix, it is reasonable to speculate that at least one of these components is responsible for the enhanced osteogenesis. For the inorganic component of pearl, it is well-known that the dissolution and hydrolysis of $CaCO_3$ in an aqueous

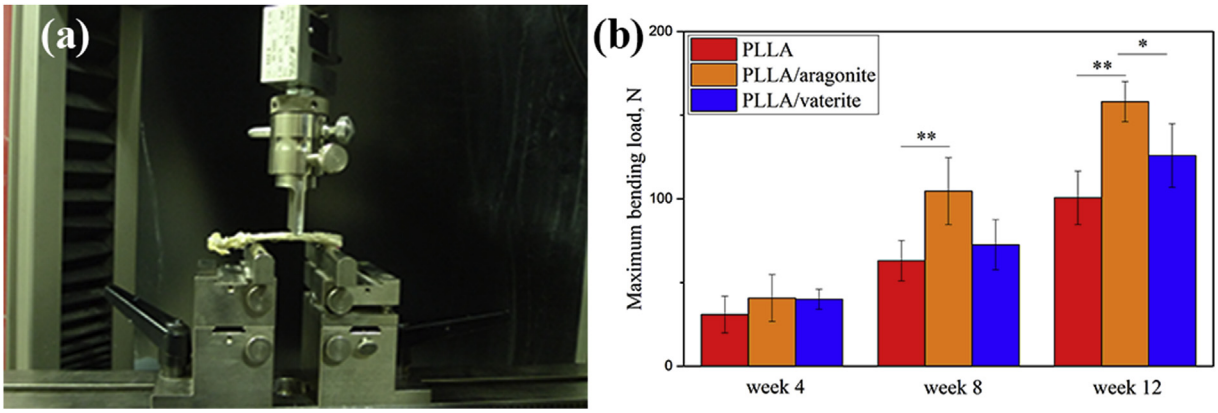

Fig. 7. (a) The experimental procedure of three-point bending test performed on rabbit forelimbs and (b) maximum bending load of the regenerated forelimbs at week 4, 8 and 12. *p < 0.05 and **p < 0.01.

environment can lead to the release of Ca^{2+} and increase of environmental pH. In previous work, we measured the alkalinity of various scaffold-soaked culture media (soaking for 1 day) and found that the pH values were in the order: PLLA/vaterite (pH ~7.4) > PLLA/aragonite (pH ~7.3) > PLLA (pH ~7.2) [36]. Moreover, the Ca^{2+} concentrations released from PLLA/aragonite and PLLA/vaterite scaffold which were immersed in phosphate buffer solution (PBS) for 7 days were measured to be ~0.26 and ~0.31 mM, respectively [37]. These results are consistent with previous finding that vaterite has a higher solubility and degradation rate than aragonite [33]. Previous literatures suggested that an alkaline microenvironment (pH 7.8–8.5) could promote osteogenesis by stimulating the activity of osteoblasts [53–55]. Meanwhile, Maeno et al. reported that 2–4 mM Ca^{2+} was suitable for the survival and proliferation of osteoblasts, while 6–8 mM Ca^{2+} was beneficial for osteoblast maturation and matrix mineralization [56]. Obviously, the environmental pH and Ca^{2+} concentration in PLLA/agragonite- or PLLA/vaterite-soaked medium are both within the tolerant ranges for osteoblasts. Thus, the dissolution of $CaCO_3$ could be partially responsible for the enhanced osteogenesis of composite scaffolds compared to pure PLLA. However, the high dissolution rate of vaterite did not lead to enhanced osteogenesis in PLLA/vaterite group compared to that in PLLA/aragonite group. Therefore, the dissolution of $CaCO_3$ does not explain the superior bone regeneration potential of PLLA/aragonite scaffold over PLLA/vaterite scaffold. This indicates that the organic matrix of aragonite pearl is likely to be more responsible for the enhanced osteogenic capacity of PLLA/aragonite scaffold compared to that of PLLA/vaterite scaffold. According to previous literatures, it is suggested that the osteogenic molecules may be contained in the WSM of nacre and pearl [23,26]. Aragonite pearl was found to possess higher content of WSM compared to vaterite pearl [35]. Thus, it is speculated that the WSM in aragonite pearl may contain more osteogenic molecules or factors which are more biologically active than that in vaterite pearl. In the future, further attention should be paid on the molecular composition of WSM in pearl in order to unveil the exact mechanism of the excellent osteogenic potential of aragonite pearl. Considering the high cost and short half-lives of growth factors such as BMP-2 and VEGF, aragonite pearl powders which contain natural osteogenic molecules within their organic matrix could be employed as functional fillers in composite scaffolds for BTE applications.

4. Conclusions

In summary, the biological performances of PLLA/aragonite and PLLA/vaterite scaffold were systematically evaluated both *in vitro* and *in vivo*. The results showed that incorporating pearl powders into PLLA scaffold enhanced *in vitro* osteogenesis and *in vivo* bone regeneration. The crystal form of pearls is critical for the biological performances of composite scaffolds. PLLA/aragonite scaffold exhibited superior osteogenic capacity over PLLA/vaterite scaffold, evidenced by the promoted cell proliferation and differentiation *in vitro* as well as the enhanced bone healing efficacy *in vivo*. Together, PLLA/aragonite scaffold is considered as a potential bone substitute material for BTE applications.

CRediT authorship contribution statement

Qianli Huang: Data curation, Formal analysis, Writing - original draft, Writing - review & editing. **Yuansheng Liu:** Data curation, Formal analysis. **Zhengxiao Ouyang:** Data curation, Formal analysis. **Qingling Feng:** Supervision, Writing - review & editing.

Declaration of competing interest

The authors declare that they have no known competing financial interests or personal relationships that could have appeared to influence the work reported in this paper.

Acknowledgments

The authors gratefully acknowledge the financial support from the China Postdoctoral Science Foundation (2018M630909 and 2019T120711).

Appendix A. Supplementary data

Supplementary data to this article can be found online at https://doi.org/10.1016/j.bioactmat.2020.06.018.

References

[1] R. Quarto, M. Mastrogiacomo, R. Cancedda, S.M. Kutepov, V. Mukhachev, A. Lavroukov, E. Kon, M. Marcacci, Repair of large bone defects with the use of autologous bone marrow stromal cells, N. Engl. J. Med. 344 (5) (2001) 385–386.
[2] V. Viateau, G. Guillemin, V. Bousson, K. Oudina, D. Hannouche, L. Sedel, D. Logeart-Avramoglou, H. Petite, Long-bone critical-size defects treated with tissue-engineered grafts: a study on sheep, J. Orthop. Res. 25 (6) (2007) 741–749.
[3] M.C. Gebhardt, D.I. Flugstad, D.S. Springfield, H.J. Mankin, The use of bone allografts for limb salvage in high-grade extremity osteosarcoma, Clin. Orthop. Relat. Res. (270) (1991) 181–196.
[4] S. Verrier, M. Alini, E. Alsberg, S. Buchman, D. Kelly, M. Laschke, M. Menger, W. Murphy, J. Stegemann, M. Schütz, Tissue engineering and regenerative approaches to improving the healing of large bone defects, Eur. Cell. Mater. 32 (2016) 87–110.
[5] K.S. Griffin, K.M. Davis, T.O. McKinley, J.O. Anglen, T.-M.G. Chu, J.D. Boerckel, M.A. Kacena, Evolution of bone grafting: bone grafts and tissue engineering strategies for vascularized bone regeneration, Clin. Rev. Bone Miner. Metabol. 13 (4) (2015) 232–244.
[6] C.R. Black, V. Goriainov, D. Gibbs, J. Kanczler, R.S. Tare, R.O. Oreffo, Bone tissue engineering, Current Molecular Biology Reports 1 (3) (2015) 132–140.

[7] L. Roseti, V. Parisi, M. Petretta, C. Cavallo, G. Desando, I. Bartolotti, B. Grigolo, Scaffolds for bone tissue engineering: state of the art and new perspectives, Mater. Sci. Eng. C 78 (2017) 1246–1262.

[8] H. Ma, C. Feng, J. Chang, C. Wu, 3D-printed bioceramic scaffolds: from bone tissue engineering to tumor therapy, Acta Biomater. 79 (2018) 37–59.

[9] C. Zhou, C. Deng, X. Chen, X. Zhao, Y. Chen, Y. Fan, X. Zhang, Mechanical and biological properties of the micro-/nano-grain functionally graded hydroxyapatite bioceramics for bone tissue engineering, Journal of the Mechanical Behavior of Biomedical Materials 48 (2015) 1–11.

[10] I. Denry, L.T. Kuhn, Design and characterization of calcium phosphate ceramic scaffolds for bone tissue engineering, Dent. Mater. 32 (1) (2016) 43–53.

[11] M. Santoro, S.R. Shah, J.L. Walker, A.G. Mikos, Poly (lactic acid) nanofibrous scaffolds for tissue engineering, Adv. Drug Deliv. Rev. 107 (2016) 206–212.

[12] T. Nie, L. Xue, M. Ge, H. Ma, J. Zhang, Fabrication of poly (L-lactic acid) tissue engineering scaffolds with precisely controlled gradient structure, Mater. Lett. 176 (2016) 25–28.

[13] S. Kuttappan, D. Mathew, M.B. Nair, Biomimetic composite scaffolds containing bioceramics and collagen/gelatin for bone tissue engineering-A mini review, Int. J. Biol. Macromol. 93 (2016) 1390–1401.

[14] P. Gupta, M. Adhikary, M. Kumar, N. Bhardwaj, B.B. Mandal, Biomimetic, osteoconductive non-mulberry silk fiber reinforced tricomposite scaffolds for bone tissue engineering, ACS Appl. Mater. Interfaces 8 (45) (2016) 30797–30810.

[15] K. Rezwan, Q. Chen, J. Blaker, A.R. Boccaccini, Biodegradable and bioactive porous polymer/inorganic composite scaffolds for bone tissue engineering, Biomaterials 27 (18) (2006) 3413–3431.

[16] C. Wang, Q. Zhao, M. Wang, Cryogenic 3D printing for producing hierarchical porous and rhBMP-2-loaded Ca-P/PLLA nanocomposite scaffolds for bone tissue engineering, Biofabrication 9 (2) (2017) 025031.

[17] W. Tang, D. Lin, Y. Yu, H. Niu, H. Guo, Y. Yuan, C. Liu, Bioinspired trimodal macro/micro/nano-porous scaffolds loading rhBMP-2 for complete regeneration of critical size bone defect, Acta Biomater. 32 (2016) 309–323.

[18] W.L. Murphy, M.C. Peters, D.H. Kohn, D.J. Mooney, Sustained release of vascular endothelial growth factor from mineralized poly (lactide-co-glycolide) scaffolds for tissue engineering, Biomaterials 21 (24) (2000) 2521–2527.

[19] F. Ren, X. Wan, Z. Ma, J. Su, Study on microstructure and thermodynamics of nacre in mussel shell, Mater. Chem. Phys. 114 (1) (2009) 367–370.

[20] E. Lopez, B. Vidal, S. Berland, S. Camprasse, G. Camprasse, C. Silve, Demonstration of the capacity of nacre to induce bone formation by human osteoblasts maintained in vitro, Tissue Cell 24 (5) (1992) 667–679.

[21] D.W. Green, H.-J. Kwon, H.-S. Jung, Osteogenic potency of nacre on human mesenchymal stem cells, Mol. Cell. 38 (3) (2015) 267.

[22] M. Lamghari, P. Antonietti, S. Berland, A. Laurent, E. Lopez, Arthrodesis of lumbar spine transverse processes using nacre in rabbit, J. Bone Miner. Res. 16 (12) (2001) 2232–2237.

[23] P. Westbroek, F. Marin, A marriage of bone and nacre, Nature 392 (6679) (1998) 861.

[24] L. Bédouet, F. Rusconi, M. Rousseau, D. Duplat, A. Marie, L. Dubost, K. Le Ny, S. Berland, J. Péduzzi, E. Lopez, Identification of low molecular weight molecules as new components of the nacre organic matrix, Comp. Biochem. Physiol. B Biochem. Mol. Biol. 144 (4) (2006) 532–543.

[25] M. Lamghari, M. Almeida, S. Berland, H. Huet, A. Laurent, C. Milet, E. Lopez, Stimulation of bone marrow cells and bone formation by nacre: in vivo and in vitro studies, Bone 25 (2) (1999) 91S–94S.

[26] M. Rousseau, L. Pereira-Mouriès, M.-J. Almeida, C. Milet, E. Lopez, The water-soluble matrix fraction from the nacre of Pinctada maxima produces earlier mineralization of MC3T3-E1 mouse pre-osteoblasts, Comp. Biochem. Physiol. B Biochem. Mol. Biol. 135 (1) (2003) 1–7.

[27] E.M. Gerhard, W. Wang, C. Li, J. Guo, I.T. Ozbolat, K.M. Rahn, A.D. Armstrong, J. Xia, G. Qian, J. Yang, Design strategies and applications of nacre-based biomaterials, Acta Biomater. 54 (2017) 21–34.

[28] M. Xu, Y. Li, H. Suo, Y. Yan, L. Liu, Q. Wang, Y. Ge, Y. Xu, Fabricating a pearl/PLGA composite scaffold by the low-temperature deposition manufacturing technique for bone tissue engineering, Biofabrication 2 (2) (2010) 025002.

[29] Y.-L. Yang, C.-H. Chang, C.-C. Huang, W.M.-W. Kao, W.-C. Liu, H.-W. Liu, Osteogenic activity of nanonized pearl powder/poly (lactide-co-glycolide) composite scaffolds for bone tissue engineering, Bio Med. Mater. Eng. 24 (1) (2014) 979–985.

[30] X. Zhang, X. Du, D. Li, R. Ao, B. Yu, B. Yu, Three dimensionally printed pearl powder/poly-caprolactone composite scaffolds for bone regeneration, Journal of Biomaterials Science, Polymer Edition 29 (14) (2018) 1686–1700.

[31] X. Li, X. Yang, X. Liu, W. He, Q. Huang, S. Li, Q. Feng, Calcium carbonate nanoparticles promote osteogenesis compared to adipogenesis in human bone-marrow mesenchymal stem cells, Prog. Nat. Sci.: Materials International 28 (5) (2018) 598–608.

[32] J. Fricain, R. Bareille, F. Ulysse, B. Dupuy, J. Amedee, Evaluation of proliferation and protein expression of human bone marrow cells cultured on coral crystallized in the aragonite or calcite form, J. Biomed. Mater. Res. 42 (1) (1998) 96–102.

[33] D.B. Trushina, T.V. Bukreeva, M.V. Kovalchuk, M.N. Antipina, $CaCO_3$ vaterite microparticles for biomedical and personal care applications, Mater. Sci. Eng. C 45 (2014) 644–658.

[34] H.Y. Ma, I.S. Lee, Characterization of vaterite in low quality freshwater-cultured pearls, Mater. Sci. Eng. C 26 (4) (2006) 721–723.

[35] Y. Ma, S. Berland, J.-P. Andrieu, Q. Feng, L. Bédouet, What is the difference in organic matrix of aragonite vs. vaterite polymorph in natural shell and pearl? Study of the pearl-forming freshwater bivalve mollusc Hyriopsis cumingii, Mater. Sci. Eng. C 33 (3) (2013) 1521–1529.

[36] Y. Liu, Q. Huang, Q. Feng, 3D scaffold of PLLA/pearl and PLLA/nacre powder for bone regeneration, Biomed. Mater. 8 (6) (2013) 065001.

[37] Y. Liu, Q. Huang, A. Kienzle, W. Müller, Q. Feng, In vitro degradation of porous PLLA/pearl powder composite scaffolds, Mater. Sci. Eng. C 38 (2014) 227–234.

[38] Z. Wang, Y. Xu, Y. Wang, Y. Ito, P. Zhang, X. Chen, Enhanced in vitro mineralization and in vivo osteogenesis of composite scaffolds through controlled surface grafting of L-lactic acid oligomer on nanohydroxyapatite, Biomacromolecules 17 (3) (2016) 818–829.

[39] X. Liu, P.X. Ma, Polymeric scaffolds for bone tissue engineering, Ann. Biomed. Eng. 32 (3) (2004) 477–486.

[40] S.J. Hollister, Porous scaffold design for tissue engineering, Nat. Mater. 4 (7) (2005) 518.

[41] C.M. Murphy, M.G. Haugh, F.J. O'Brien, The effect of mean pore size on cell attachment, proliferation and migration in collagen–glycosaminoglycan scaffolds for bone tissue engineering, Biomaterials 31 (3) (2010) 461–466.

[42] V. Karageorgiou, D. Kaplan, Porosity of 3D biomaterial scaffolds and osteogenesis, Biomaterials 26 (27) (2005) 5474–5491.

[43] M. Ni, B.D. Ratner, Nacre surface transformation to hydroxyapatite in a phosphate buffer solution, Biomaterials 24 (23) (2003) 4323–4331.

[44] J.O. Hollinger, J.C. Kleinschmidt, The critical size defect as an experimental model to test bone repair materials, J. Craniofac. Surg. 1 (1) (1990) 60–68.

[45] L.M. Pineda, M. Büsing, R.P. Meinig, S. Gogolewski, Bone regeneration with resorbable polymeric membranes. III. Effect of poly (L-lactide) membrane pore size on the bone healing process in large defects, J. Biomed. Mater. Res. 31 (3) (1996) 385–394.

[46] E.W. Bodde, P.H. Spauwen, A.G. Mikos, J.A. Jansen, Closing capacity of segmental radius defects in rabbits, J. Biomed. Mater. Res. 85 (1) (2008) 206–217.

[47] D. Zhou, K. Zhao, Y. Li, F. Cui, I. Lee, Repair of segmental defects with nano-hydroxyapatite/collagen/PLA composite combined with mesenchymal stem cells, J. Bioact. Compat Polym. 21 (5) (2006) 373–384.

[48] M. Walton, N.J. Cotton, Long-term in vivo degradation of poly-L-lactide (PLLA) in bone, J. Biomater. Appl. 21 (4) (2007) 395–411.

[49] H.K. Makadia, S.J. Siegel, Poly lactic-co-glycolic acid (PLGA) as biodegradable controlled drug delivery carrier, Polymers 3 (3) (2011) 1377–1397.

[50] M. Van Dijk, D. Tunc, T. Smit, P. Higham, E. Burger, P. Wuisman, In vitro and in vivo degradation of bioabsorbable PLLA spinal fusion cages, J. Biomed. Mater. Res. 63 (6) (2002) 752–759.

[51] D.A. Bushinsky, Acid-base imbalance and the skeleton, Eur. J. Nutr. 40 (5) (2001) 238–244.

[52] T. Guda, J.A. Walker, B.E. Pollot, M.R. Appleford, S. Oh, J.L. Ong, J.C. Wenke, In vivo performance of bilayer hydroxyapatite scaffolds for bone tissue regeneration in the rabbit radius, J. Mater. Sci. Mater. Med. 22 (3) (2011) 647–656.

[53] H. Pan, Y. Shen, C. Wen, S. Peng, W.W. Lu, Role of pH—the essential step for osteoporotic bone regeneration, Bone 47 (2010) S444.

[54] J. Tan, D. Wang, H. Cao, Y. Qiao, H. Zhu, X. Liu, Effect of local alkaline microenvironment on the behaviors of bacteria and osteogenic cells, ACS Appl. Mater. Interfaces 10 (49) (2018) 42018–42029.

[55] Q. Li, D. Wang, J. Qiu, F. Peng, X. Liu, Regulating the local pH level of titanium via Mg–Fe layered double hydroxides films for enhanced osteogenesis, Biomaterials Science 6 (5) (2018) 1227–1237.

[56] S. Maeno, Y. Niki, H. Matsumoto, H. Morioka, T. Yatabe, A. Funayama, Y. Toyama, T. Taguchi, J. Tanaka, The effect of calcium ion concentration on osteoblast viability, proliferation and differentiation in monolayer and 3D culture, Biomaterials 26 (23) (2005) 4847–4855.